5AND97-2533C 5AND--97-2533C

ELECTROTHERMAL ACTUATORS FABRICATED IN FOUR-LEVEL PLANARIZED SURFACE-MICROMACHINED POLYCRYSTALLINE SILICON

John H. Comtois*, M. Adrian Michalicek*, and Carole Craig Barron**

*U.S. Air Force Phillips Laboratory, KAFB, NM 87117

**U.S. Department of Energy, Sandia National Laboratories, KAFB, NM 87117

SUMMARY

This paper presents the results of tests performed on a variety of electrothermal microactuators and arrays of these actuators fabricated in the SUMMiT process at the U. S. Department of Energy's Sandia National Laboratories [1]. These results are intended to aid designers of thermally actuated mechanisms, and they apply to similar actuators made in other polysilicon MEMS processes such as the MUMPS process [2]. Measurements include force and deflection versus input power, maximum operating frequency, effects of long term operation, and ideal actuator and array geometries for different applications' force requirements. Also, different methods of arraying these actuators together are compared. It is found that a method using rotary joints, enabled by the advanced features of the SUMMiT fabrication process, is the most efficient array design. The design and operation of a thermally actuated stepper motor is explained to illustrate a useful application of these arrays.

Keywords: microactuators, electrothermal, SUMMiT, micromotors, polysilicon, surface micromachining

ELECTROTHERMAL MICROACTUATOR THEORY

The basic device studied in this research is a single-material actuator which deflects at its tip due to unequal thermal expansion of its constituent parts. A typical 'U' shaped electrothermal actuator is shown in Fig. 1. The entire actuator is released from the substrate except at the two anchor points. It consists of two arms of uneven width joined at the end opposite the anchors to form the "U" shape. The wider 'cold' arm has a narrow flexure at the base (anchor side) to permit that side to bend. This physical arrangement constrains the actuator tip to move laterally in an arcing motion towards the cold arm side when the structure is unevenly heated [3,4]. In the simplest method of actuation a current is passed through the actuator via the anchors and the higher current density in the narrower 'hot' arm results in greater ohmic heating, causing it to expand in length more than the wider cold arm.

DISTRIBUTION OF THIS DOCUMENT IS UNLIMITED



MASTER

DISCLAIMER

This report was prepared as an account of work sponsored by an agency of the United States Government. Neither the United States Government nor any agency thereof, nor any of their employees, make any warranty, express or implied, or assumes any legal liability or responsibility for the accuracy, completeness, or usefulness of any information, apparatus, product, or process disclosed, or represents that its use would not infringe privately owned rights. Reference herein to any specific commercial product, process, or service by trade name, trademark, manufacturer, or otherwise does not necessarily constitute or imply its endorsement, recommendation, or favoring by the United States Government or any agency thereof. The views and opinions of authors expressed herein do not necessarily state or reflect those of the United States Government or any agency thereof.

DISCLAIMER

Portions of this document may be illegible in electronic image products. Images are produced from the best available original document. The flexure on the cold arm is sized so that it does not expand significantly compared to the hot arm, even though it experiences the same current density. This is not only because it is shorter, but also because at either end there are sinks for the heat it generates, preventing it from becoming as hot as the hot arm. Similar structures have also been actuated by heating one of the arms from an external heat source. Expansion could also be caused by exothermic chemical reaction with a coating on one of the arms, or by laser heating, for example.

Deflection caused by expansion of the hot arm is defined as forward deflection. Backwards deflection can also be achieved by momentarily overheating the hot arm, then letting it cool. As the hot arm heats to a plastic state, the restoring force of the bent flexure causes the actuator to retract from its maximum deflection by deforming the hot arm, typically by bowing it, thus decreasing its straight line anchor-to-tip length. The hot arm retains this new shape when the heat is removed, and the actuator deflects backwards from its initially fabricated position when it cools. Backbending allows two other operating modes: the actuator can deliver a static backwards force, or it can be operated in the forward direction from a new starting position. When this type of actuator encounters a resistance to forward bending, the hot arm is likely to bow even before the plastic temperature is reached, which limits the amount of force that can be delivered. When backbending, however, the hot arm is pulling along its length rather than pushing, so it will not bow, and can therefore deliver more force.

A 250 μ m long actuator is capable of 19 μ m of deflection when unloaded, and can deliver up to 19 μ N of force in forward deflection. Arrays of actuators allow the generation of many 10's of μ N of force. Most importantly, these actuators operate in a current and voltage regime which is directly compatible with standard CMOS electronics, e.g. 0 to 12 volts at 0 to 5 mA, depending on the geometry and maximum deflection or force desired. This simple actuator can be fabricated in any MEMS process that includes at least one releasable layer, preferably a current-carrying layer to allow simple ohmic heating actuation. This makes it amenable to a wide variety of MEMS processes, and it has been tried in the LIGAMUMPS process [5], electroplated nickel [6], in bulk etched CMOS, and most extensively in the MUMPS process [4,7]. This paper examines actuators made in a four-layer surface-micromachined polysilicon process with a planarized upper layer. Such a sophisticated process is not necessary to create a single actuator, but it does enable a wider variety of designs for joining single actuators together into arrays, and more sophisticated applications.

The actuators themselves could be made in other ways if other process steps were available. For instance, it would be unnecessary to have the cold arm be wider if the two arms could be made uneven in resistivity, perhaps by

patterned doping. Better insulation of the heat-generating region of the hot arm would make it more energy efficient [6]. Ideally the hot arm would heat with a minimum of heat loss, but would also cool instantly when the current was removed to increase the maximum operating frequency.

SUMMIT FABRICATION PROCESS

The devices presented in this paper were fabricated in the SUMMiT (Sandia Ultra-planar Multi-level MEMS Technology) [1,8]. As in other surface-micromachined polysilicon processes, the devices are formed in SUMMiT by the alternate deposition of structural polysilicon layers and sacrificial oxide layers, over a base nitride layer. Additional features of the SUMMiT process include a planarized uppermost polysilicon layer and a special 'pin joint' for rotary couplings [9]. The upper polysilicon layer is not planarized directly; instead, the oxide layer directly beneath it is chemical-mechanically polished before the final polysilicon layer is deposited. This removes any topographical features in the uppermost polysilicon layer due to patterns in the underlying layers, eliminating mechanical interference. The pin joint is formed by a timed wet etch through a hole patterned in the first polysilicon layer. The wet etch undercuts the edges of the hole, and subsequent depositions of oxide and the second polysilicon layer form an inverted mushroom of polysilicon through the hole. Thus at the pin joint there is second polysilicon both above and below the first polysilicon layer, as shown in Fig. 2. When the oxide is etched away, the resulting structure is free to rotate (if the hole is round), but is constrained from pulling out of the hole. The devices were release etched for 20 minutes in a 1:1 mix of HF and HCL, then dried in supercritical carbon dioxide process.

The complexity of the micromachines which can be manufactured in a given process is a function of the number of independent layers of structural polysilicon the technology provides. So although the actuators presented in this paper require only one releasable structural layer, complex applications of them usually require more. Geared mechanisms, for example, require two independent levels of structural polysilicon, one to form the hubs and the other the moving gears. Reduction-geared mechanisms require two independent, non-interfering levels in order to form working two-level gear trains. The SUMMiT process provides these features, as well as one-micron feature sizes for more intricate mechanisms.

SINGLE ACTUATOR TEST RESULTS

This section reports the results of tests performed on single actuators of 90 slightly different geometries. The variations are used to identify the ideal geometry for applications requiring different deflections and forces. The

actuators fall into four length categories: 150, 200, 250 and 300 microns long. Within those categories are variations of hot arm width, flexure length and the width of the gap between the two arms. All of the actuators are formed in a composite layer formed from the first and second polysilicon layers (Poly-1 and Poly-2) stacked directly together with no intervening oxide layer. The resulting 2.5 micron thick polysilicon layer puts the overall device resistance into a range that makes it CMOS-compatible, i.e. a cold resistance in the range of 0.5 to 3 kilohms.

The actuators are instrumented to measure their output force at different deflections. This instrumentation consists of beams of different widths for the actuators to press against, with scales to measure deflection, as shown in Fig. 3. Based on results of actuators made in the MUMPS process [10] and mathematical modeling of the bending beams, copies of each type of actuator were fabricated with bending beams of different widths to ensure that each actuator would be bracketed by test beams that were neither too stiff nor too flexible to get useful results. A beam too stiff does not deflect far enough to get a reliable measurement; too flexible a beam and the actuator reaches nearly the same maximum deflection it would reach with no test beam. Ideally the test beam deflects far enough to get a measurable deflection, but not so far that the actuator is losing force bending its own flexure rather than delivering maximum force to the test beam.

Actuators with no instrument load were also tested for their deflection versus power characteristics, to determine which geometrical variations produced the largest unloaded deflection at the lowest input power. The actuators were tested under static conditions by advancing the deflection in 1 μ m increments then stopping to record the voltage and current. The accuracy of reading the deflection scales was \pm 0.25 μ m. Each actuator was deflected until it showed the initial signs of back-bending, i.e. the loss of forward deflection due to plastic deformation of the hot arm. In actual use, the actuators are typically operated at no more than 80% of this maximum power. Table 1 lists the dimensions of actuators of different lengths that achieved the highest deflection at the lowest input power. These dimensions may also be ideal for lightly loaded actuators (<1 μ N), though no tests were conducted at this light a load. Figure 4 shows the deflection versus input power responses of the actuators listed in Table 1.

Table 1. Best dimensions for unloaded or lightly loaded actuators. All dimensions are in microns.

Length	Hot arm width	Flexure length	Gap width	Max. deflection	Max. power, mW
150	1	30	1.5	9	13
200	1.5	50	1.5	13	21
250	1.5	80	1.5	19	32

300	2	75	1.5	22	42

Analyzing the results of all the unloaded actuator tests, it was seen to be generally best to use the thinnest possible hot arm. This lowers the power requirement by raising the overall resistance of the hot arm. Since little force is being delivered by the actuator, the thinness of the hot arm does not cause premature bowing. Although actuators with a longer flexure deflected a micron or two more than the ones listed in Table 1, these actuators also drew more power at each deflection. This could be due to heating of the flexure, resulting in a slight overall increase in power at each deflection setting, despite the fact that a longer flexure is easier to bend as evidenced by the slightly greater maximum deflection.

The 300 µm long actuators exhibited an oscillation caused by the hot arm bowing down and touching the substrate. When the substrate is contacted the arm cools and shrinks up out of contact, whereupon it heats again and the cycle repeats. The result was a vibration of the arm with a D.C. voltage input. This effect was also sometimes observed in the 250 µm long actuators, though only at the higher deflections.

Force versus input power measurements were taken on actuators instrumented with force test beams, as shown in Fig. 3. The measurements were carried out in the same quasi-static manner outlined above. Because hot arm oscillation affected the longest actuators, they were not tested for force. It turns out that the actuator geometries that give the best deflection versus power performance when unloaded do not give the best power consumption performance when loaded. Table 2 lists the dimensions of actuators which showed the best overall power versus force performance for heavily loaded actuators. Performance for a given length improved as the flexure length improved, up to the point where the flexure was about 25% of the length of the actuator. Beyond this the performance under a load would decrease despite the fact that a longer flexure is easier to bend. The reason is that the longer flexures tended to bend into a shallow "S" shape instead of a simple curve, allowing the actuator tip to back away from the load beam.

Figure 5 shows the force versus input power for the actuators listed in Table2. From this figure it can be seen that longer actuators can deliver more overall force, but also at higher input power. The 200 µm long actuator had a flexure that was 25% of its length rather than 20% like the other two, and also a wider gap. The actuators listed in the tables are the best performers for a given length, not actuators of a given series, i.e. not all have the same gap or

flexure length ratio. So the 200 μm actuator in Fig. 5 shows as good a power performance as the 150 μm actuator for a given force.

Table 2. Ideal dimensions for heavily loaded actuator, for best power versus force performance. Geometric dimensions in microns.

Length	Hot arm width	Flexure length	Gap width	Max. Force, μN	Max. power, mW
150	1.5	30	1.5	8	18
200	2	50	2	9	21
250	2.5	50	1.5	11	33

Table 3 lists the dimensions of the actuators that delivered the maximum force at any power. The highest forces were delivered by the actuator types with a wider hot arm and a larger gap between arms. The wider hot arm provides more expanding material, so would be expected to deliver more force; and a wider gap increases the leverage of the hot arm for bending the actuator. However, the wider hot arm is itself harder to bend, and a wider gap increases the force by decreasing the overall deflection. So both of these design choices for obtaining higher forces are a tradeoff with maximum deflection.

For this type of actuator, more force can be delivered at lower deflections, since the actuator must also bend its own flexure, which requires more force the farther it bends. Also, the hot arm delivers less force by bowing more out of line at higher deflections, thus pressing less on the tip of the actuator. Figure 6 shows the force versus input power for actuators listed in Table 3. Comparing these results to those of Fig. 5, note that the power consumption is higher for a given output force, but the maximum force available is much higher.

Table 3. Dimensions of actuators that delivered the highest force at any power. Geometric dimensions in microns.

Length	Hot arm width	Flexure length	Gap width	Max. Force, μN	Max. power, mW
150	2	30	2	10	25
200	2.5	65	2	14	35

250	3	75	2	19	40

It was expected and observed that a longer actuator will deflect farther when unloaded and will deliver more force. But this trend stops when the hot arm gets long enough to sag onto the substrate, which occurred regularly with actuators of 300 μ m length. Dimples can be used to support the hot arm, but although they provide less heat loss area for oscillation, they also add a stick-slip motion which makes the deflection of the actuator less predictable.

The maximum operating frequency for these actuators is here defined to be the frequency of a square wave input signal at which the actuator no longer reaches the full deflection it achieves in DC operation at the same peak voltage as the square wave. These actuators typically had a maximum frequency of between 0.4 and 1.6 kHz, with longer actuators having lower maximum frequencies. However, the actuators were still observed to have a deflection greater than 2 µm at much higher frequencies. For example, a 200 µm long actuator had a maximum frequency of 1.48 kHz at full deflection, but still showed about 2 µm of deflection at 13 kHz, which is useful for many optical applications. The results of measurements on the actuators listed in Table 1 are summarized in Table 4. Note that the entry for "1/2 motion" denotes a deflection halfway between full deflection and the position of the actuator where motion stops with increasing drive frequency which is roughly at 2/3 of full deflection.

Table 4. Operating frequency characteristics for unloaded actuators of different lengths.

Length, μm	Deflection, µm	Maximum frequency	Frequency at ½ motion	Frequency where motion stops
150	7	1.6 kHz	7 kHz	24 kHz
200	8	1.5 kHz	7 kHz	30 kHz
250	12	800 Hz	6 kHz	11 kHz
300	12	490 Hz	5.7 kHz	42 kHz

Actuators of the same overall length had roughly the same frequency characteristics, with the maximum frequency increasing slightly with decreasing flexure length. The frequency values at ½ and zero motion are less exact, as it was more difficult to determine these deflections visually. At drive frequencies above the "zero deflection" frequency the actuator remains at roughly 2/3 deflection, for the 50% duty cycle square wave signal

used. Also, above that frequency the deflection can be set by adjusting the peak voltage or the pulse width. This characteristic is due to the inability of the hot arm to cool between cycles, so it averages the input power pulses [4].

The actuators were capable of higher frequency operation when loaded. For example, a 200 μ m long actuator under a load of 7 μ N had a maximum frequency of 2.5 kHz, although a mutual resonance with the force test beam led to chaotic deflections at some frequencies. Resonance modes were not detected when testing the unloaded actuators. The actuator deflection remained constant with increasing frequency up to the maximum frequency, then it decreased smoothly down to the deflection where motion stopped as the input frequency continued to increase. Actuators connected to other structures also have higher operating frequencies due to the added heat loss path of conduction to the connected structure [11].

These actuators are probably best suited for use in applications where they are not operated continuously, e.g. for positioning mechanisms or self-assembly. However, a few of the actuators and arrays were operated for a large number of cycles to determine if this mode of operation would degrade their performance. Because of limited equipment, a concerted program of testing could not be carried out, so only a few results are presented here, to indicate the general trends of the actuators and arrays.

The long term tests were conducted in an open bay lab and a condensate, probably water, collected in beads around the flexure and underneath the hot arm of the array actuators. The beads eventually coalesced and wicked under the actuator cold arm, causing it to stick to the substrate. This moisture appeared regardless of the drive frequency, and reached detrimental proportions within 24 hours. For most tests accumulated moisture caused the array mechanism to stick down eventually, although the hot arms kept bowing with the drive signal without breaking.

A 200 µm long actuator under a load of 7 µN was operated for 980 million cycles at 2 kHz. At the end of this test the actuator was still reaching its full deflection, although it had eroded a 0.5 µm divot into the force test beam where it struck (refer to Fig. 2), which occasionally trapped the actuator tip. Even though the actuator still reached full deflection, it had acquired a slight bow in the hot arm. Also, power consumption decreased 6% as the resistance of the device decreased over time. This may have been due to annealing of the hot arm. All of the actuators exhibited a 5-10% decrease in cold resistance after being operated for 10 seconds at nearly their maximum voltage.

One array of 8 actuators was operated for 54.5 million cycles at 800 Hz with no change in operation. The array was delivering a force of 18.2 μ N to a test beam at an input power of 41 mW. In another example, an array driving

a stepper motor operated for 83 million cycles before the yoke stuck to the substrate, leaving the actuator hot arms still flexing. It could not be determined if the yoke became stuck due to moisture.

ACTUATOR ARRAY FORCE TEST RESULTS

Arrays consisted of a single row of 2 to 12 actuators connected by four different mechanisms. Die space constraints made it necessary to choose only three actuator geometries and employ them in all the array types, and this before the ideal actuator geometry was known from the single actuator tests. The result was that only one of the three actuator designs turned out to be of an ideal geometry, so only tests on those actuators are reported. The actuator chosen was 200 μ m long, with a hot arm width of 2 μ m, gap of 1.5 μ m, and a flexure 50 μ m long. Based on the single actuator test results, this geometry will have the best input power versus force characteristics for this length of actuator.

Three of the four types of array mechanisms or 'yokes' were named for their connection schemes: flexural, pinslot, and rotating joint. The fourth arraying scheme, called 'cascaded pushers', does not physically tie the actuators together. Yoke-type arrays can perform several functions. They are primarily used to add together the force of several actuators, since obtaining more force by making larger actuators quickly runs into a length limit as seen previously. Yokes also allow the actuators to be conveniently coupled to the driven structure. Close-up views of the four styles of array linkages are shown in Fig. 7a-d.

The flexural yoke (Fig. 7a) is the style used successfully in the past [12]. In this type of array the actuators are attached with short flexures to a common yoke. The flexures are designed to bend easily in the direction of the actuator length, and to remain rigid in the deflection direction. The flexures are required so that the actuator can pivot. Advantages of this yoke are its compactness, its ability to be fabricated in a single releasable layer, and ease of attachment. A disadvantage is that some force is lost in bending the yoke flexures. That loss can be decreased by making the flexures longer, but this uses more area and results in a more compliant connection to the driven structure.

The pin-slot type, shown in Fig. 7b, was an attempt to address the force lost in the bending the flexural yoke. This approach works, and motors using this style of array were successfully operated. However, the pin-slot yoke has the disadvantage that it is supported by dimples instead of the actuators. In testing this led to stick/slip motion

and these arrays were the first to fail from stiction. Also, the yoke is free to rock and the actuator pins can slip out of it, even with a poly-3 cover to capture the pins. There is also some deflection lost due to the necessary gap between the pins and the slot walls.

The rotary joint type, shown in Fig. 7c, was by far the most successful, delivering the most force per input power to the test beams in all cases. It also has the advantage of being compact. The rotary motion eliminates force losses, and less than 1 µm of deflection is lost in the play of the rotary joints. The yoke is also supported by the actuators instead of on dimples. However, this particular design relies on the pin joint fabrication and planarization capabilities of the SUMMiT process. A similar yoke could be built in other processes, but would require three releasable structural layers.

The cascaded pusher approach was also successful at eliminating force losses, but only at smaller deflections and in smaller arrays. This is because required gaps between actuators force the actuators farther back from the force application point to bend more before contacting the preceding actuators, so this is not practical for large arrays. Also, when these arrays are used in a back-bending mode, not all of the actuators may backbend exactly the same amount, leaving gaps in the chain. The uneven backbending seen in these tests was due to resistive losses in the power busses resulting in uneven current flow in all the actuators. Future array designs in SUMMiT will require wider busses since the process does not include a metal layer. In designs with metal conductors uneven backbending has not been observed in arrays. The cascaded pusher array design can be fabricated in a single releasable layer, though it works best for low deflection applications with four or fewer actuators.

Yokes can be used to combine the motion of the individual actuators, eliminating the arcing motion of single actuators. For example, actuators in a single row connected to a yoke will result in a motion of the yoke that is mostly linear and tangential to the arcing motion of the individual actuators. This arrangement also exhibits a slight sideways motion as the actuators expand in length and go through their arc. One way to eliminate this slight lateral motion is to use two opposing rows of actuators joined by a compliant "Y" shaped yoke as shown in Fig 8. The compliant "Y" arrangement absorbs the lateral motion of the expanding actuators, resulting in a purely linear motion of the overall yoke [12].

In general, each actuator requires some force just to bend itself, so for the lowest power consumption it is best to use the fewest number of actuators that can deliver the required force and deflection. Figure 9 shows force versus power for the four different array styles, with eight actuators in each of the arrays. The SUMMiT actuators turned

out to have more force than previously tested polysilicon actuators. This difference was small enough to remain within the range of force test beams used for the single actuator tests, but the force difference summed over a large array placed the array's total force outside the range of test beams chosen. Since the force of the arrays was underestimated no meaningful force results could be determined, only a comparison of power consumption at a given deflection. The arrays would just move to their maximum deflection with very little additional power consumption over unloaded arrays. Figure 9 clearly shows that the rotary yoke outperforms the other three types by consuming roughly half the power for the same deflection. This indicates that the rotary array should be able to deliver much more force.

ARRAY APPLICATION EXAMPLE

As an example of how these actuator arrays might be used, a rotary stepper motor was built which drives a multi-layer gear train, shown in Fig. 10. The motor was designed without prior knowledge of the maximum possible array deflection in the SUMMiT process, so a two-level rotor gear was used to match the possibly small actuator array deflection to the tooth pitch of the gears which are automatically generated by a library routine set up by Sandia. A similar drive motion has also been tried with a linear stepper motor where the rotor is replaced by a toothed rack.

The motor is operated by two arrays set at 90 degrees to each other. The smaller array engages the drive pawl with the rotor, and the larger array moves the rotor [7]. The smaller array is typically back-bent before the first operation so that the pawl engages the rotor when the power is off, to act as a brake. The main array can have any number of actuators depending on the load to be driven. On previous motors, arrays of up to 60 actuators were successfully operated [12]. The drive voltage for the small array is set so that when power is applied, the pawl teeth just barely clear the rotor teeth. The voltage for the main array is set so that it will deflect exactly 1 tooth spacing. This makes for the smoothest motion, because the teeth will be perfectly aligned for the next stroke when the pawl retracts. In operation, the two arrays are driven with square waves that are 90 degrees out of phase. This results in the following four-part motion, starting from an unpowered state: power on the main array pulls the rotor 1 tooth

distance, power on the small array disengages the pawl, main array power is removed and the pawl retracts 1 tooth spacing, small array power is removed, re-engaging the pawl with the rotor.

As a result of this study, it will be possible to design arrays that can drive the larger gear teeth directly. However, smaller teeth create more steps per revolution for more accurate angular positioning. Of course the actuators can be positioned at any deflection, so it is possible to get sub-tooth resolution by disengaging the pawl after positioning. In this situation, it would be better to have the small array engage the pawl when power is applied, rather than vice-versa as done in this design. Then the pawl will not engage the rotor and move it when power is removed. However, this will leave the rotor free to rotate due to other torques in the system. Another option is to have no teeth on the pawl or rotor, there is sufficient sidewall roughness to drive the rotor for low-torque applications.

ACKNOWLEDGEMENT

The portion of this work done at Sandia National Labs was supported by the U.S. Dept. of Energy under contract DE-AC04-94AL85000. Sandia is a multiprogram laboratory operated by Sandia Corporation, a Lockheed Martin Company, for the U.S. Dept. of Energy.

REFERENCES

- 1. R. Nasby, J. Sneigowski, J. Smith, S. Montague, C. Barron, W. Eaton and P. McWhorter, "Application of chemical-mechanical polishing to planarization of surface-micromachined devices," *Technical Digest, Solid State Sensors and Actuators Workshop*, Hilton Head, SC, 3-6 June 1996, pp. 48-53.
- 2. D. Koester, R. Mahedevan, and K. Marcus, *Multi-User MEMS Processes (MUMPS) Introduction and Design Rules*, rev. 3, Oct 1994, MCNC MEMS Technology Applications Center, 3021 Cornwallis Road, Research Triangle Park, NC, 27709.
- 3. H. Guckel, J. Klein, T. Christenson, K. Skrobis, M. Laudon, and E. Lovell, "Thermo-magnetic Metal Flexure Actuators," *Technical Digest, Solid State Sensors and Actuators Workshop*, Hilton Head, SC, 13-16 June 1992, pp. 73-75.
- 4. J. Comtois, V. Bright, and M. Phipps, "Thermal Micro-actuators for Surface-micromachining Processes," *Proc. SPIE: Micromachined Devices and Components*, vol. 2642, 23-24 October 1995, pp. 10-21.
- 5. MCNC Web Page: http://www.mcnc.org, or MCNC Electronic Technologies Division, PO Box 12889, 3021 Cornwallis Road, RTP, NC, 27709-2889.
- 6. L. Field, D. Buriesci, P. Robrish, and R. Ruby, "Micro-machined 1x2 Optical Fiber Switch," *Proc. Transducers '95/Eurosensors IX*, Stockholm, Sweden, 1995, pp. 344-347.

- 7. J. H. Comtois and V. M. Bright, "Applications for surface micromachined polysilicon thermal actuators and arrays," *Sensors and Actuators*, vol. A 58, pp. 19-25, 1997.
- 8. Sandia National Laboratory Web Page: http://www.mdl.sandia.gov
- 9. E. J. Garcia and J. J. Sniegowski, "Surface micromachined microengine as the driver for micromechanical gears," *Proc. Transducers* '95/Eurosensors IX, Stockholm, Sweden, 1995, pp. 365-368.
- 10. J. R. Reid, V. M. Bright, and J. H. Comtois, "Force measurements of polysilicon thermal micro-actuators," *Proc. SPIE: Micromachined Devices and Components II*, vol. 2882, pp. 296-306, 14-15 Oct. 1996.
- 11. D. Sene, J. Grantham, V. Bright, and J. Comtois, "Development and Characterization of Micro-mechanical Gratings for Optical Modulation," *Proc. IEEE MEMS-96 Workshop*, San Diego, CA, 11-15 Feb. 1996, pp. 222-227.
- 12. John H. Comtois, "Structures and Techniques For Implementing and Packaging Complex, Large Scale Microelectromechanical Systems Using Foundry Fabrication Processes," Ph.D. dissertation, Air Force Inst. of Tech., ref. AFIT/DS/ENG/96-04, May 1996.

Figure Captions

- Figure 1. Schematic top view of an electrothermal actuator showing the main features. The actuator is released from the substrate everywhere except at the anchors.
- Figure 2. Cross section of a pin joint exposed by Focused Ion Beam. The 'pin' is the three horizontal layers of lighter-colored polysilicon joined at the center of the photo. The two lower horizontal levels are the actual pin, and the uppermost light colored poly connects the pin to another structure off to the right of the photo. There is no change in color to show the join of the poly levels, but it occurs at the lower edge of the upper oxide layer, which has a hole cut through it to form the via between the pin and the uppermost poly. The lower, darker polysilicon layer is also composed of two polysilicon layers joined together. A very thin layer of oxide separates the light and dark poly layers within the joint, so the pin is free to rotate when released. This joint is similar to the ones used in the arrays studied in this paper, except this photo does not show a planarized uppermost polysilicon layer.
- Figure 3. Four independent 150 μ m long actuators, each instrumented with deflection scales and two test beams for measuring force in both forward and backward deflection. The test beam width is varied to measure different force ranges. The scales are marked in 2 μ m increments.
- Figure 4. Deflection versus power for the actuators listed in Table 1. Maximum voltages applied to the 150, 200, 250, and 300 μ m long actuators were 8.3, 9, 13, and 13.7 V respectively. Error in deflection readings is +/- 0.25 μ m.
- Figure 5. Force versus power for the actuator types listed in Table 2. These actuators were selected for a balance of high force with the least amount of input power. A tolerance of \pm 0.25 μ m in reading the beam deflections leads to an error of \pm 0.07 μ N for the 150 μ m long actuator and 0.45 μ N for the 200 and 250 μ m long actuators which were measured with a wider test beam.
- Figure 6. Force versus power for the actuator types listed in Table 3. These actuators were selected for maximum force at any input power. A tolerance of +/- 0.25 μm in reading the beam deflections leads to an error of +/- 0.07 μN for the 150 μm long actuator and 0.45 μN for the 200 and 250 μm long actuators which were measured with a wider test beam.
- Figure 7. Close-up views of the four variations of actuator arrays studied in this paper. Each array is instrumented with force test beams on either side to measure forward and reverse deflection forces. The pusher array (d) has a straight scale measured in 2 μ m increments. The yoke style arrays (a through c) have vernier scales reading in 0.2 μ m increments, but actual measurements were taken with a straight scale with 2 μ m increments on a reticle.
- Figure 8. A 2-sided flexural array fabricated in the MUMPS process. This arrangement of actuators cancels any length-wise motion of the actuators, resulting in purely linear motion of the array yoke at the guide bearing at the top of the photo. The actuators are 220 μ m long.
- Figure 9. Force versus input power for the four types of arrays. Each array combined the force of eight $200\mu m$ long actuators. A tolerance of +/- 0.25 μm in reading the beam deflections leads to an error of +/- 1.4 μN for these force measurements.
- Figure 10. Rotary stepper motor driven by two thermal actuator arrays. The main two-level gear adapts thermal actuator stroke to tooth pitch of standard, software-generated Sandia gears. The upper level gears are fabricated in planarized Poly-3. The main array can be seen at the bottom of the photo, and part of the smaller array which engages the drive pawl can be seen at the left side of the photo. Both arrays are of the flexural type.

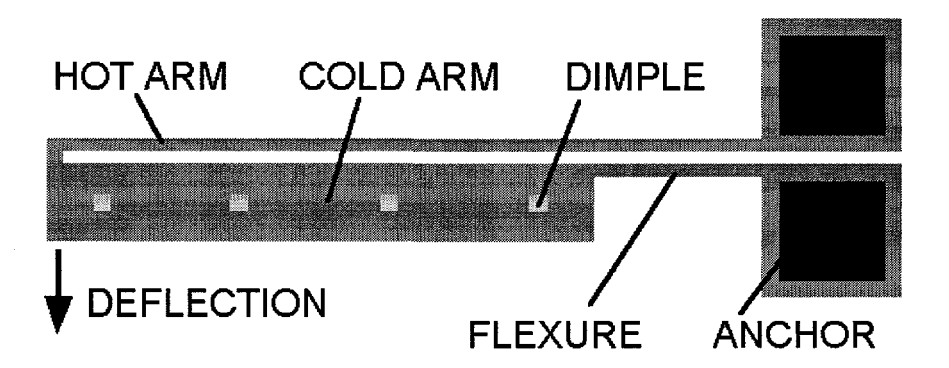


Figure 1. Schematic top view of an electrothermal actuator showing the main features. The actuator is released from the substrate everywhere except at the anchors.

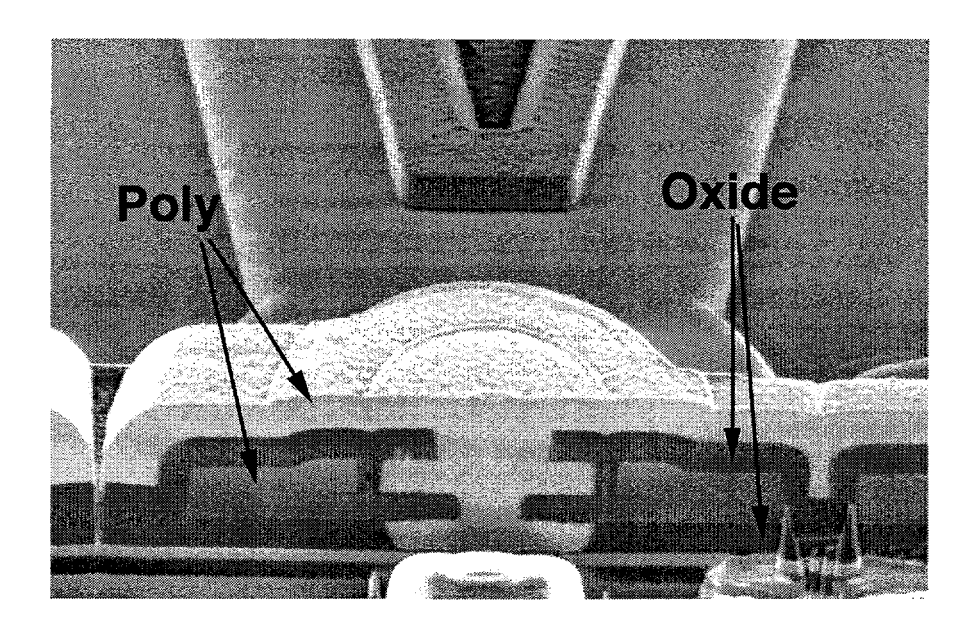


Figure 2. Cross section of a pin joint exposed by Focused Ion Beam. The 'pin' is the three horizontal layers of lighter-colored polysilicon joined at the center of the photo. The two lower horizontal levels are the actual pin, and the uppermost light colored poly connects the pin to another structure off to the right of the photo. There is no change in color to show the join of the poly levels, but it occurs at the lower edge of the upper oxide layer, which has a hole cut through it to form the via between the pin and the uppermost poly. The lower, darker polysilicon layer is also composed of two polysilicon layers joined together. A very thin layer of oxide separates the light and dark poly layers within the joint, so the pin is free to rotate when released. This joint is similar to the ones used in the arrays studied in this paper, except this photo does not show a planarized uppermost polysilicon layer.

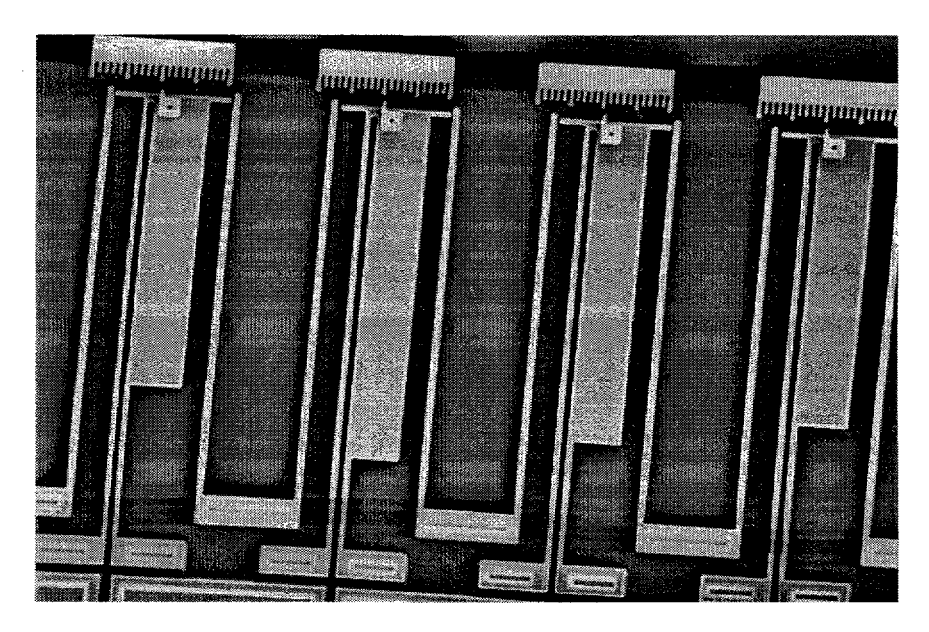


Figure 3. Four independent 150 μ m long actuators, each instrumented with deflection scales and two test beams for measuring force in both forward and backward deflection. The test beam width is varied to measure different force ranges. The scales are marked in 2 μ m increments.

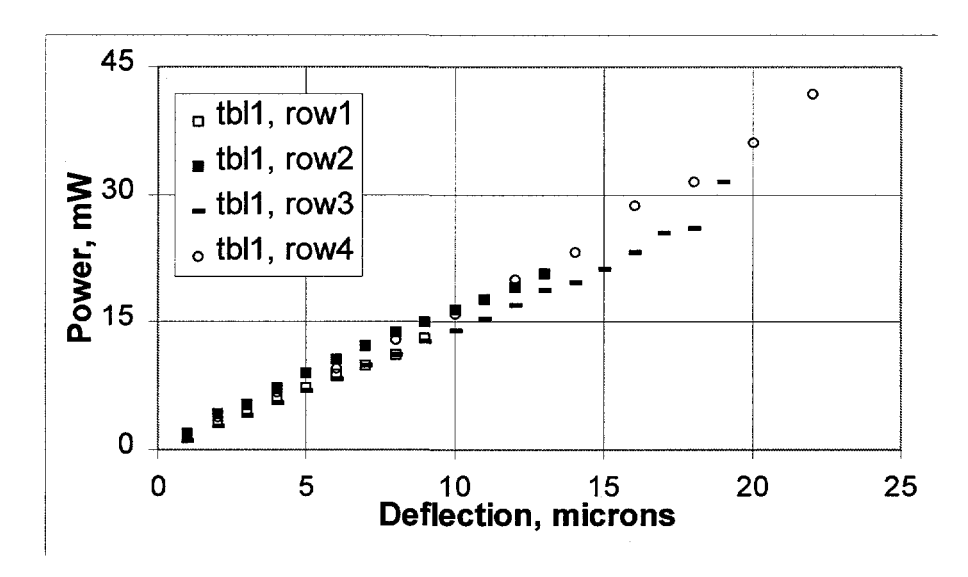


Figure 4. Deflection versus power for the actuators listed in Table 1. Maximum voltages applied to the 150, 200, 250, and 300 μ m long actuators were 8.3, 9, 13, and 13.7 V respectively. Error in deflection readings is +/- 0.25 μ m.

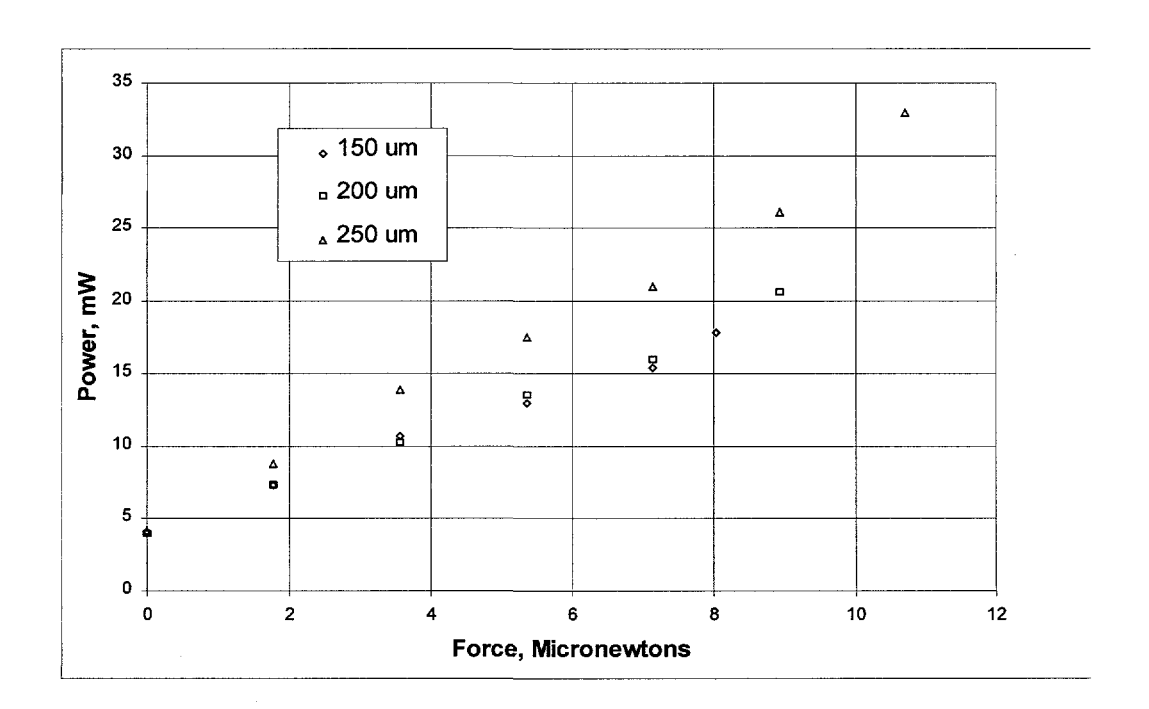


Figure 5. Force versus power for the actuator types listed in Table 2. These actuators were selected for a balance of high force with the least amount of input power. A tolerance of +/- 0.25 μ m in reading the beam deflections leads to an error of +/- 0.07 μ N for the 150 μ m long actuator ,and 0.45 μ N for the 200 and 250 μ m long actuators which were measured with a wider test beam.

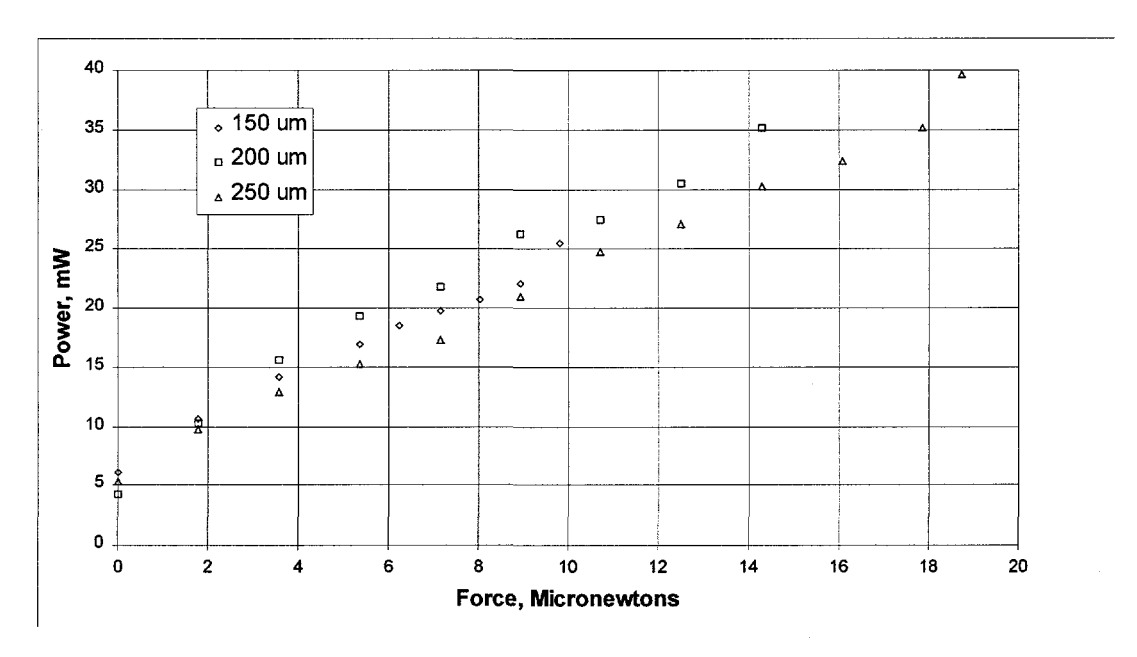


Figure 6. Force versus power for the actuator types listed in Table 3. These actuators were selected for maximum force at any input power. A tolerance of +/- 0.25 μ m in reading the beam deflections leads to an error of +/- 0.07 μ N for the 150 μ m long actuator ,and 0.45 μ N for the 200 and 250 μ m long actuators which were measured with a wider test beam.

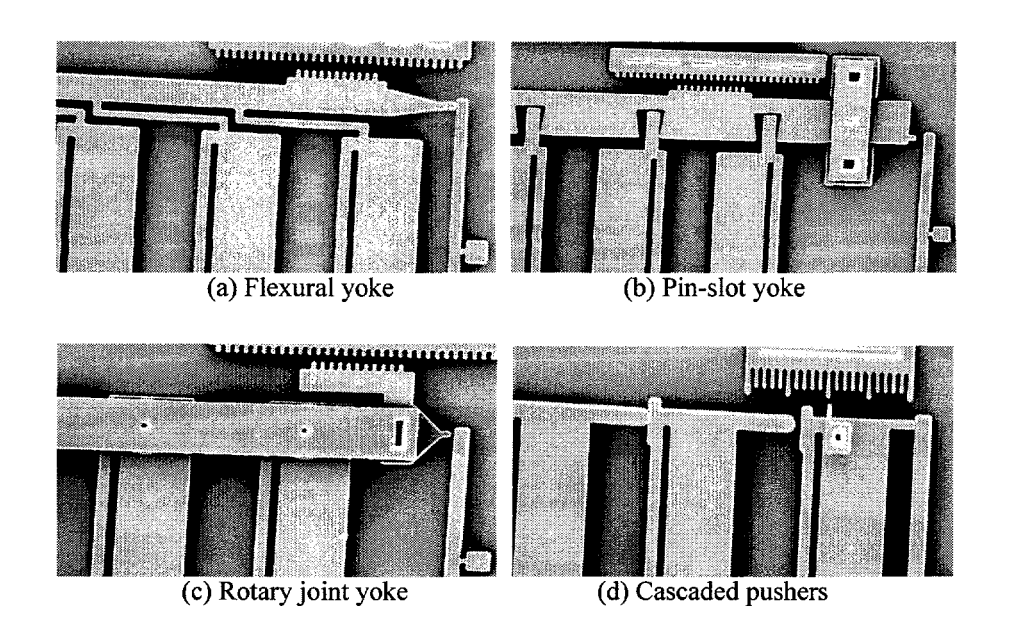


Figure 7. Close-up views of the four variations of actuator arrays studied in this paper. Each array is instrumented with force test beams on either side to measure forward and reverse deflection forces. The pusher array (d) has a straight scale measured in 2 μ m increments. The yoke style arrays (a through c) have vernier scales reading in 0.2 μ m increments, but actual measurements were taken with a straight scale with 2 μ m increments on a reticle.

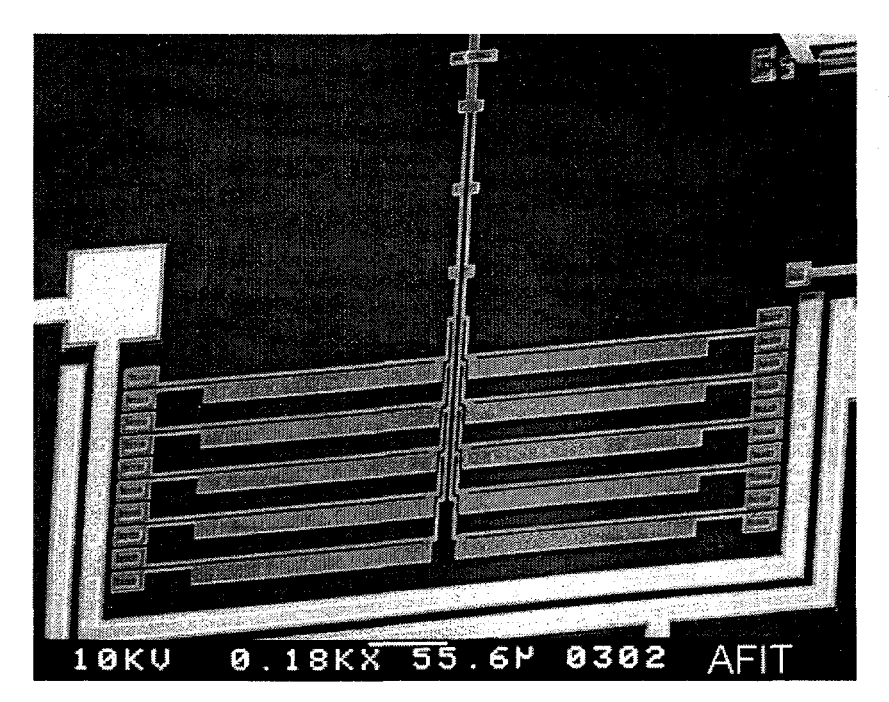


Figure 8. A 2-sided flexural array fabricated in the MUMPS process. This arrangement of actuators cancels any length-wise motion of the actuators, resulting in purely linear motion of the array yoke at the guide bearing at the top of the photo. The actuators are $220 \mu m \log$.

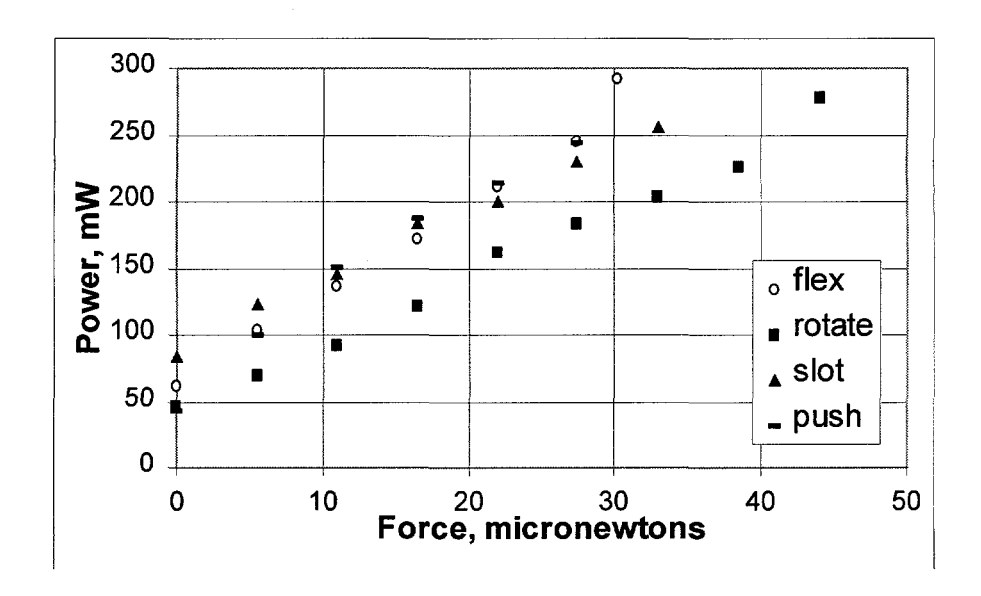


Figure 9. Force versus input power for the four types of arrays. Each array combined the force of eight 200 μ m long actuators. A tolerance of +/- 0.25 μ m in reading the beam deflections leads to an error of +/- 1.4 μ N for these force measurements.

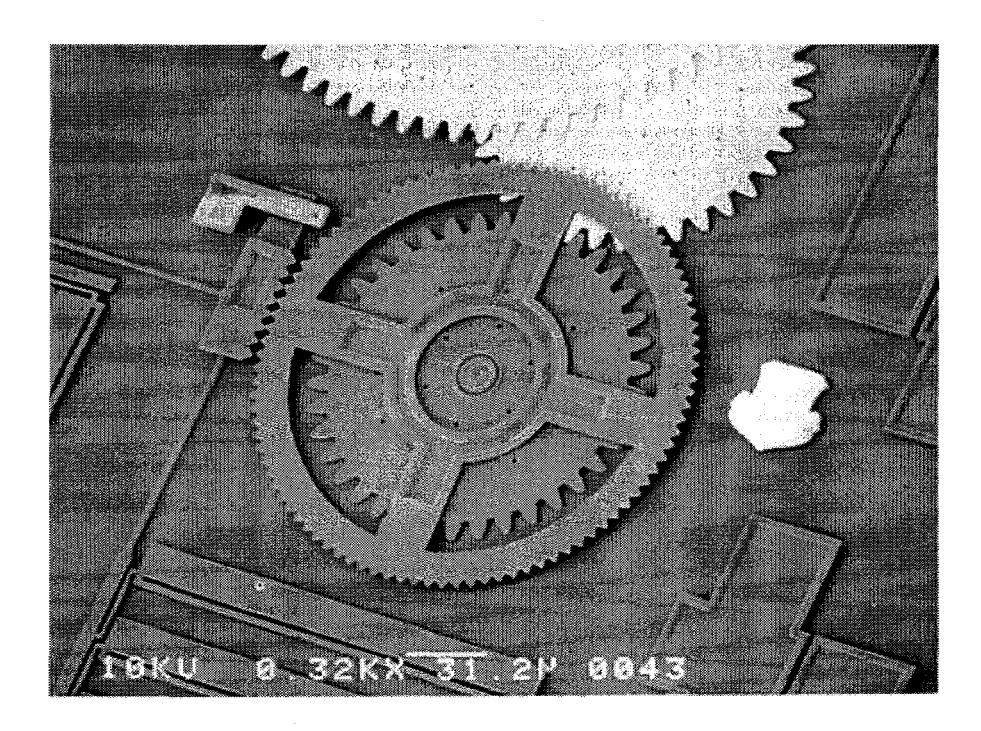


Figure 10. Rotary stepper motor driven by two thermal actuator arrays. The main two-level gear adapts thermal actuator stroke to tooth pitch of standard, software-generated Sandia gears. The upper level gears are fabricated in planarized Poly-3. The main array can be seen at the bottom of the photo, and part of the smaller array which engages the drive pawl can be seen at the left side of the photo. Both arrays are of the flexural type.